Earthq Eng & Eng Vib (2021) 20: 791-802 **DOI**: https://doi.org/10.1007/s11803-021-2052-5

Mechanical property of U-Shaped 65Mn steel bumpers for seismic base isolation

Han Miao[1†], Wang Yuandong[2‡], Du Hongkai[1§,4*] and Cui Xiangdong[3£]

1. *Beijing University of Civil Engineering and Architecture, Beijing 102612, China*
2. *BHB Consulting Engineers, Salt Lake City, Utah 84115, USA*
3. *Jining Huiyuan Huazhu Architectural Design Co., Ltd, Jining 272000, China*
4. *University of Utah, Salt Lake City, Utah 84112, USA*

Abstract: This study proposes a novel U-shaped 65Mn steel bumper as the displacement restraining device for base-isolated structures with laminated elastomeric rubber bearings. A series of bumpers with different geometric parameters were designed and tested under monotonic and cyclic quasi-static loading protocols. The experimental results from a total of 232 specimens were analyzed to develop an analytical model to calculate the backbone curve and the maximum elastic restoring force for U-shaped 65Mn bumpers. Thus, the analytical equations to calculate the elastic, hardening, and unloading stiffness of U-shaped 65Mn bumpers, as well as their maximum elastic restoring force, are validated by using an additional ten groups of bumpers with varying radiuses. These analytical equations can accurately predict the mechanical parameters of U-shaped 65Mn steel bumpers for a design purpose.

Keywords: U-shaped bumper; base isolation; experimental; mechanical properties; analytical model

1 Introduction

Flexible base isolators elongate the fundamental period of base-isolated structures, which reduces superstructures′ responses (Aiken *et al*., 1989; Wang and Ibarra, 2015; Zhou *et al*., 2018). However, under near-fault ground motions (GMs) and GMs with significant pulses, the base level of structures with elastomeric bearings can exhibit large horizontal displacement, which may induce severe superstructure responses when pounding against moat walls or adjacent structures occurs, damaging isolation bearings (Mavronicola *et al*., 2017; Pant and Wijeyewickrema, 2014). This pounding may lead to significant damage to structures that could increase the annual frequency of collapse (Ibarra and Krawinkler, 2005; Ye *et al*., 2009) or even cause collapses during a seismic event (Wang *et al*., 2016; Wang *et al*., 2019).

Increasing the damping of the isolation layer (e.g., implementing U-shaped dampers) can effectively reduce the deformation of the isolation layer. The feasibility of using U-shaped ordinary steel plates as damping devices and their mechanical properties have been investigated in previous studies. Seismic energy was dissipated during the deformation and yielding of U-shaped steel plates (Tagawa and Gao, 2012; Oh *et al*., 2013; Xie *et al*., 2018). Suzuki *et al*. (2005) conducted a series of experimental tests to investigate the velocity and temperature dependence of mechanical properties for U-shaped steel dampers. Deng *et al*. (2013, 2015) developed and tested crawler steel dampers that could be installed on bridges. Also, analytical equations were derived to estimate the damper strength, based on equilibrium and compatibility equations in addition to the virtual work principle. The optimal configuration of improved U-shaped dampers was obtained, which can significantly improve dampers′ bi-directional performance compared to traditional U-shaped dampers. Du *et al*. (2014) proposed three calculation methods for U-shaped steel plates, namely, the correction coefficient method, the diagram method, and the finite element method. All three methods have their own advantages and can be applied comprehensively to projects to achieve a high degree of accuracy. Jiao *et al*. (2015) conducted dynamic loading tests to evaluate ultimate plastic deformation capacities, hysteretic behaviors of U-shaped dampers, and the effects of initial temperature.

Another method used to control the displacement of an isolation layer is the employment of bumpers/stoppers. Displacement limitation by bumpers is a method that

Correspondence to: Du Hongkai, Beijing University of Civil Engineering and Architecture, Beijing 102612, China
Tel: +86-10-68322526
E-mail: duhongkai@bucea.edu.cn
[†]Professor; [‡]Project Engineer; [§]Assocaite Professor; [*]Visiting Professor; [£]Engineer

Supported by: National Science Foundation of China for the Financial Support for This Research under Grant Nos. 51378047 and 51408027
Received August 10, 2019; **Accepted** March 19, 2020

was proposed by Han and Zhou (1999) to control the horizontal displacement of the isolation layer. This device is meant to assist base isolated structures to resist the effects of extreme earthquakes or near-fault earthquakes. The structural mechanism is designed to install soft bumpers with a gap in based-isolated superstructures as a second defense, which does not change the structural system of the main structure. U-shaped bumpers have no structural effect due to frequent earthquakes (i.e., a 63% probability of exceedance in 50 years). However, their superior strength can efficiently limit the horizontal displacement of base isolated structures due to severe earthquakes (2% in 50 years or rare) by pounding with the superstructures and increasing the stiffness of the isolation layer. Skinner *et al*. (1993) proposed to restrain the horizontal seismic displacement of base-isolated governmental buildings in New Zealand through the use of stoppers or resilient buffers. Guerreiro and Azevedo (1996) analyzed the effect of bumpers in limiting the base displacements for isolated structures. The results showed that erecting bumpers was a viable solution to minimize the predesigned gap distance between isolated structures and moat walls. Masroor and Mosqueda (2012a, 2012b) performed a series of earthquake simulating experiments to assess the performance limit states of seismically isolated buildings pounding against moat walls. Thus, a nonlinear inelastic force-based impact model for rubber bumpers was used to numerically simulate the pounding that takes place between base isolated structures and adjacent buildings that have a small gap distance.

Different types of bumpers were investigated in previous studies such as elastic-gap devices (Dicleli, 2008), rubber shock absorbers (Polycarpou *et al*., 2013), spring bumpers (Du and Han, 2014), and X-shaped elastic-plastic steel shear keys (Liu *et al*., 2015). However, most of these bumpers require support members such as boundary fixity, and none of the above-mentioned ordinary dampers and bumpers can be reused due to their small elastic deformation capacity. A new generation of displacement restraining devices, such as the U-shaped 65Mn steel bumper, is proposed in this study. The 65Mn steel bumper has a material yield strength that is three times as greater than regular structural steel and is able to remain elastic under an extreme load. Thus, U-shaped steel plate bumpers can be directly installed at the base beams of isolation in one or two directions without boundary fixity, as shown in Fig. 1 (Han and Li, 2006). The main objective of this study is to experimentally evaluate the mechanical properties of U-shaped 65Mn steel bumpers. Thus, analytical equations are also provided for future engineering applications after validation by applying experimental results.

2 Specimen and experiment design

2.1 Test Specimens

The geometric configuration of a U-shaped 65Mn steel bumper is shown in Fig. 2. The main design parameters include circular section radius (R), straight section length (L), straight section width (B), and plate thickness (t). Forty-eight groups of U-shaped 65Mn bumpers were designed with different L, B, t, as in Table 1. Each group contains four bumpers with the

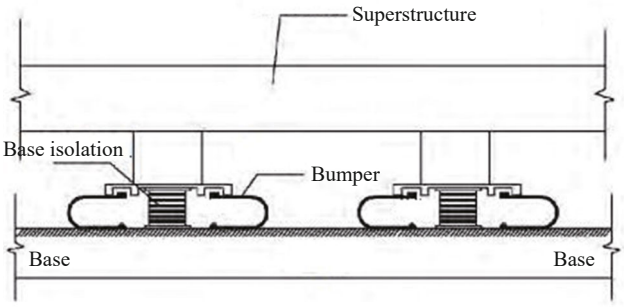

Fig. 1 Proposed installation configurations of U-shaped steel bumpers

Table 1 Design parameters of U-shaped 65Mn steel bumpers

R (mm)	L (mm)	B (mm)	t (mm)
100	150/200	60/80/120/160	6
100	150/200	60/80/120/160	8
100	150/200	60/80/120/160	10
100	150/200	60/80/120/160	12
100	150/200	60/80/120/160	14
100	150/200	60/80/120/160	16

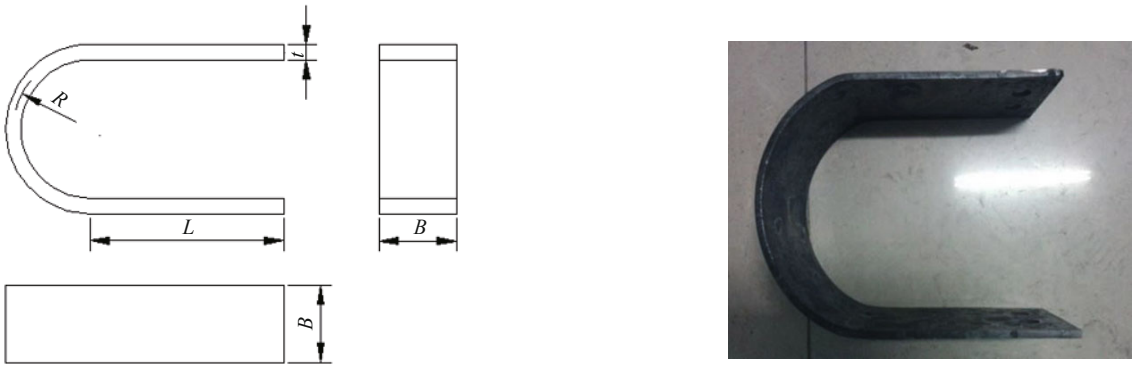

Fig. 2 Configuration and dimensions of a U-shaped steel bumper

same design parameters to record experimental results from monotonic and cyclic tests to achieve a high level of confidence.

To validate the equations regressed from the previous 48 groups of specimens, an additional 10 groups of U-shaped 65Mn steel bumpers were designed with different R (Table 2) and were tested under the same protocol. As a result, the total number of tests in this study is 232.

2.2 Material property

The tensile property of steel plate standard components for 65Mn steel bumpers was performed on a universal experimental machine (UTM) at Beijing University of Civil Engineering and Architecture. Figure 3 shows an experimental stress-strain backbone curve of a 65Mn steel standard component, which presents a high yield strength (near to 1,000 MPa) compared to the yield strength (300 – 400 MPa) of normal structural steel. However, a brittle fracture suddenly occurred when the steel component reached its ultimate strength. Table 3 summaries yield strength, ultimate strength, and yielding strain for 65Mn standard steel plates of varying thickness.

2.3 Experimental setup

Figure 4 shows the standard experimental setup for a U-shaped 65Mn steel bumper. A horizontal actuator applied static loading protocols with a loading plate that was attached to the bumper in a longitudinal direction. The bumper′s lower branch was connected to the actuator, while the upper branch was connected to a plate that was fixed by a triangular brace, horizontally, and four anchor bolts vertically. During each test, the actuator′s output force and internal displacement were recorded as the horizontal reactions of bumpers. The internal displacement of the actuator equals the relative deformation found between the upper and lower branch of the testing bumper. The surface strain of each bumper was collected by strain gauges located between the circular and straight portions of each bumper.

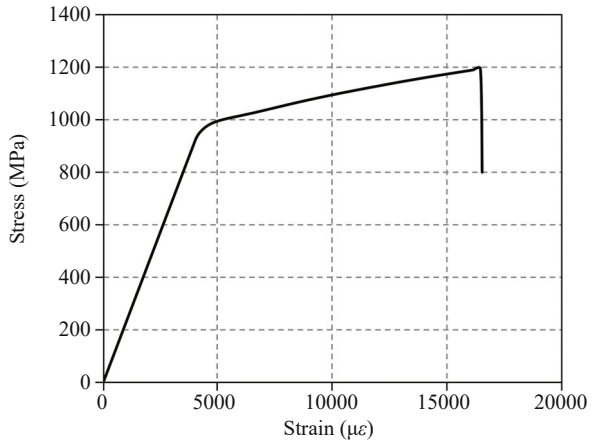

Fig. 3 Stress-strain curve of a standard steel bumper component (t = 12 mm)

Table 2 Design parameters of U-shaped 65Mn bumpers with different R

R (mm)	L (mm)	B (mm)	t (mm)
40	150	40/80	8
60	150	40/80	8
80	150	40/80	8
100	150	40/80	8
120	150	40/80	8

Table 3 Strength and strain of steel bumpers with varying thickness

Thickness t (mm)	6	8	10	12	14	16	mean
f_y (MPa)	983	1001	805	919	805	787	845
f_u (MPa)	1425	1290	1220	1213	980	937	1178
ε_y (10^{-6})	4796	4461	3911	4030	3924	3756	4096

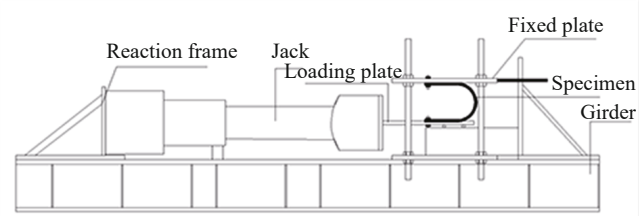

(a) Configuration of test setup

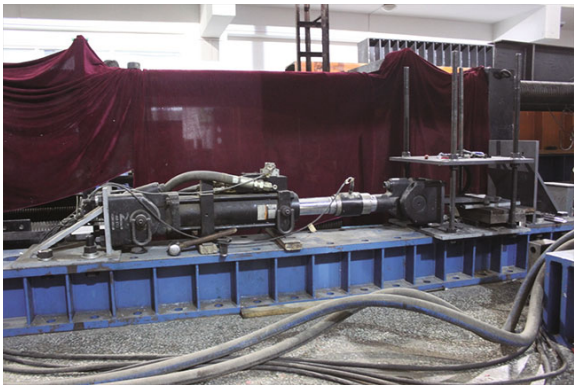

(b) Picture of test setup

(c) Detail picture of specimen and test setup

Fig. 4 U-shaped bumper test setup

2.4 Loading protocol

In each group, two specimens were loaded monotonically, while two other specimens were tested under cyclic loading protocol by using the displacement control method. The loading protocol for each specimen was divided into four levels, 10 mm, 25 mm, 50 mm, and 100 mm, with corresponding velocities of 0.1 mm/s, 0.25 mm/s, 0.5 mm/s, and 1 mm/s. The monotonic loading test is repeated once for each level. The cyclic loading test is repeated once at the first three levels and three times at the last level. Each test was designed to be stopped if any bumper brittle fracture occurred during the loading process.

3 Test result analysis

3.1 Force-deformation curves under monotonic load

SJ1 – SJ6 represent the specimens with $B =$ 80 mm, $L =$ 150 mm, but different plate thicknesses, which are $t =$ 6 mm, 8 mm, 10 mm, 12 mm, 14 mm, and 16 mm, as shown in Table 1. The force-deformation curves of specimens SJ1–SJ6 under the monotonic loading protocol are shown in Fig. 5, and the curves of specimens with other B and L are also similar. As expected, the steel material remained elastic under small deformation, while the bumper capacity increased with plate thickness. However, the elastic limit of the displacements increased with the decrease of steel plate thickness. Also, once steel bumpers reached the point of elastic-plastic deformation, significant unloading residual deformation was observed. For instance, with an extremely thick steel plate (t = 16 mm), a brittle fracture occurred in specimen SJ6 between the circular and straight portions (see Fig. 5 curve SJ6), which proved to be the thickness limit of brittle fracture for the tested R.

During the experimental tests, the deformation performance of a U-shaped steel bumper was found to be close to the bending process of a steel plate. Steel plate surface strain and stress increase with its thickness under the same bending angle. The surface material is also prone to yield with a larger amount of thickness, which internally requires a much higher applied load. A previous study (Du *et al*., 2014) proved that thickness and bend radius determine the surface strain of a steel plate, $\varepsilon = t / 2R$. ε denotes the surface strain, and R represents the bent radius. Based on their results, it can be observed that brittle fracture occurs with a higher ε in U-shaped bumpers. As a result, specimens with t = 16 mm are prone to brittle failure with the same R, and their surface strain can reach material ultimate tensile strain faster than the case with other specimens. Correspondingly, brittle fracture of U-shaped bumpers can be avoided by designing its maximum surface strain to fall below its material limit, which means limiting a bumper′s minimum bend radius (the circular section radius R) and plate thickness (t).

3.2 Force-deformation curves under cyclic load

The experimental elastic deformation limit also increases as steel plate thickness decreases under cyclic loading (Fig. 6). Significant unloading residual deformation was generated when elastic-plastic deformation occurred in the tested bumpers. The hysteretic response was found to be close under three cyclic loading protocols that displayed the same peak displacement. Thus, unloading stiffness decreases with the increase of maximum applied deformation, which indicates the occurrence of stiffness degradation under cyclic loadings. The hysteretic loops are rounded and symmetrical, but with pinching, which indicates that the U-shaped 65Mn steel bumper has limited ductility and energy dissipation capacity. It was also observed that a thicker steel plate could dissipate more seismic energy due to material yielding and plasticization.

During the experiments, steel plate bend radius decreased, with an increase in bumper deformation. A thinner steel plate and smaller bend radius leads to a larger bumper deformation when material yield strain is the same. Similar to other elastoplastic elements, the unloading stiffness of a U-shaped bumper is smaller than its elastic stiffness. In addition, a steel plate's plasticity determines energy dissipation capacity, which is controlled by bumper thickness. However, as discussed in the previous section, brittle fracture should be avoided by limiting plate thickness.

3.3 Influence of L on bumper deformation

Similar to specimens SJ1 – SJ6, the tested bumpers that have B = 80 mm, $L =$ 200 mm and different t are labeled SJ1′ – SJ6′. These specimens were tested under the same loading protocol as in section 3.1. The test results showed that the length of the straight section would not significantly modify either the effective stiffness or the peak strength of bumpers, as shown in Fig. 7.

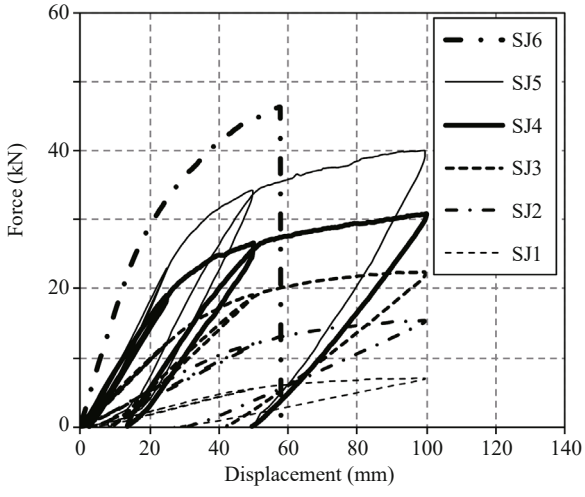

Fig. 5 Force-deformation curves of specimens SJ1 – SJ6 under monotonic load

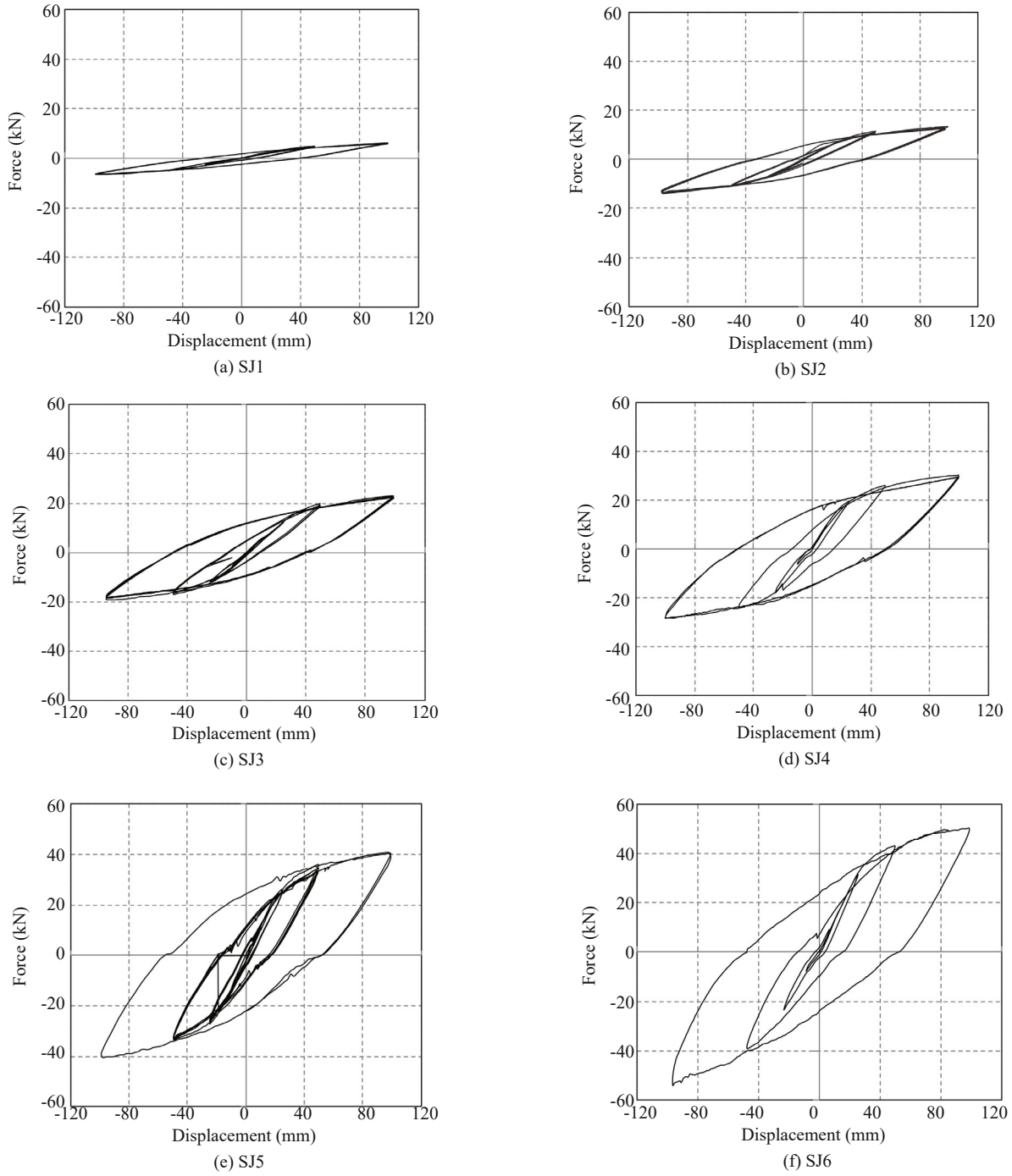

Fig. 6 Hysteretic responses of specimen SJ1 – SJ6 under horizontal cyclic load

Since the tested U-shaped bumpers have significant widths, the deformation of the specimen only occurs in the crimp direction. The straight section length determines the ultimate bumper deformation, regardless of applied load.

3.4 Force-displacement backbone curves

Figure 8 shows the backbone curves for specimens with different thicknesses under monotonic and cyclic loading protocols. With the same overall dimensions, bumpers′ elastic restoring force increases proportionally to steel plate thickness, while a thicker plate may reduce the elastic limit and the amount of plastic deformation. This indicates that an optimal plate thickness could be provided to ensure the stability of the bumpers and balance cost and dissipated energy during a seismic event.

The backbone curves for U-shaped bumpers with 65Mn steel can theoretically be divided into three portions, which are elastic, elastic-plastic, and unloading. In this study, analytical functions were obtained by fitting experimental data from forty-eight specimens into straight lines by employing the least-squares method

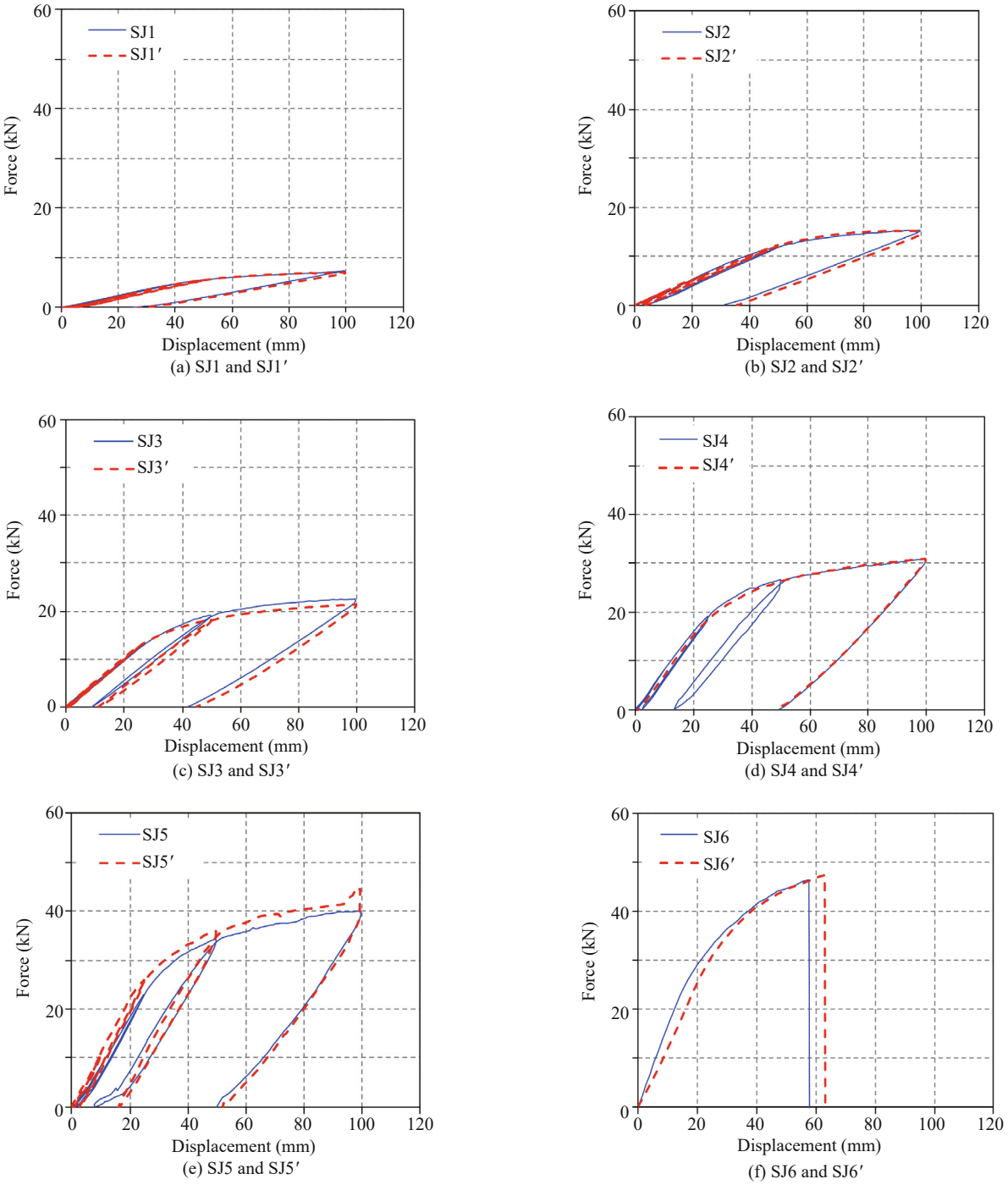

Fig. 7 Specimens force-deformation curve under monotonic load

(Fig. 9). Correspondingly, the model parameters will include elastic stiffness K_1, elastic-plastic stiffness K_2, and unloading stiffness K_3. K_2 is a tangent stiffness that considers data variations, and Δ_y represents plastic deformation. In Fig. 9, y_1 represents the elastic limit, while maximum displacement is denoted by y_2 (i.e., 100 mm). F1 and F2 represent yielding strength and ultimate strength. Some K_1 and K_3 are shown in Table 4, while the remainder can be referred to as in Cui (2015). λ represents the correction factor of elastic stiffness (see section 4.1).

3.5 Surface strain and deformation

The ratio of steel plate thickness (t) to circular section radius (R) is defined as Φ. SJ7, SJ8, SJ9 represent specimens containing different plate thicknesses (t= 12, 14, 16 mm), but the same R= 100 mm and B = 160 mm. Figure 10 shows the correlation between strain and bumper deformations under cyclic loading, which proves that applied displacement amplifies bumper surface strain. Also, the magnitude of surface strain increases with Φ. Thus, yield strain (ε) occurs

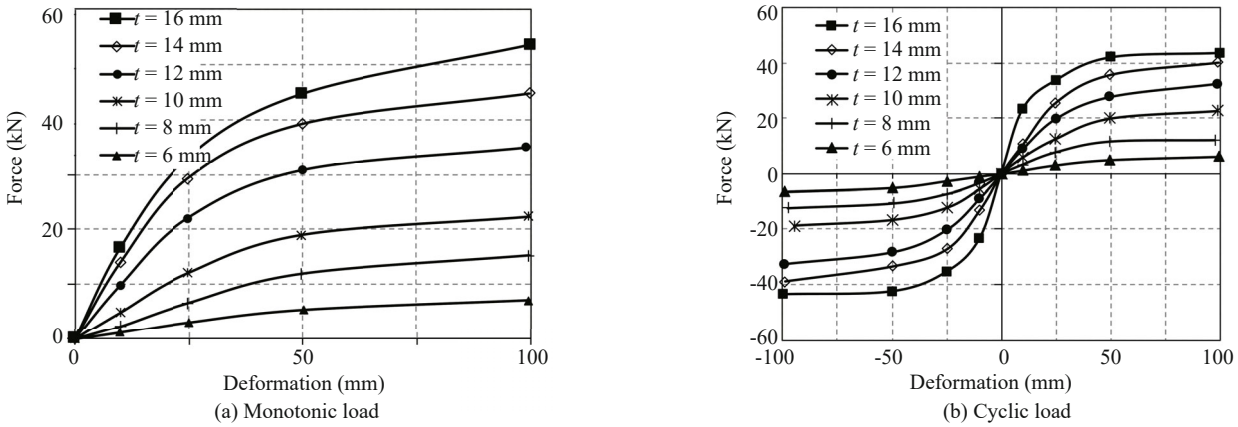

Fig. 8 Force-deformation relationships of specimens with varying plate thickness

Table 4 Stiffness of U-shape 65Mn steel bumpers (t = 8 mm, L = 150 mm)

Stiffness (N/mm)	Width, B (mm)			
	60	80	120	160
K_1	222.0	295.0	441.0	534.0
K_3	173.2	236.0	374.9	453.9
K_0	334.1	445.4	668.2	891.0
λ	0.66	0.66	0.66	0.61

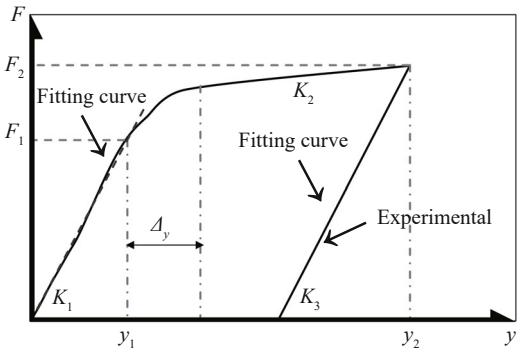

Fig. 9 Analytical force-deformation curve of U-shaped bumpers

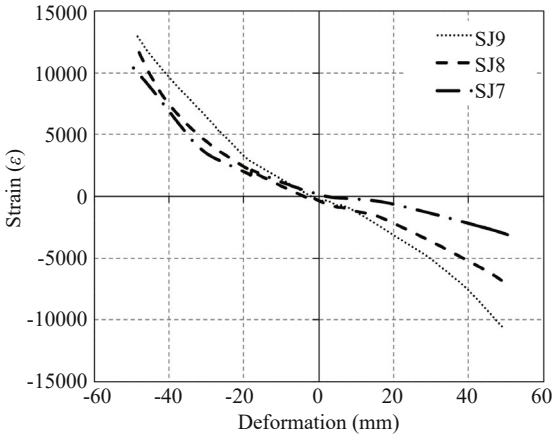

Fig. 10 Surface strain to deformation curves for specimen SJ7, SJ8, SJ9 under cyclic load

earlier, with an increase of Φ, which indicates that the curved section in U-shaped bumpers with a higher Φ is more prone to material yielding, which corresponds to the discussions found in sections 3.1 and 3.2.

4 Analytical stiffness equation

4.1 Theoretical elastic stiffness

This section establishes an analytical model for the mechanical design properties of 65Mn U-shaped bumpers. A theoretical out-of-plane elastic stiffness of a U-shaped steel bumper is defined as K_0 (Du *et al*., 2014) in Eq. (1). E denotes steel elastic modulus, and K_0 is proportional to Φ^3. The correction factor of elastic stiffness $\lambda = K_1 / K_0$ is first introduced to adjust analytical elastic stiffness, based upon a certain type of bumpers (t = 8 mm, L = 150 mm) that are listed in Table 4.

$$K_0 = \frac{EBt^3}{6\pi R^3} = \frac{EB\Phi^3}{6\pi} \tag{1}$$

A linear relationship is assumed between λ and Φ in Eq. (2) for broad application, which assumes that a, b are constants. As observed, there is no correlation between λ and B. Linear regression analyses of λ to Φ were performed with the results from 48 sets of experimental specimens. Figures 11 and 12 include all 48 experimental results from static monotonic and cyclic loading protocols, which summarize the values of $a = 0.84$, $b = -2.85$ that converts the elastic stiffness to Eq. (3).

$$\lambda = a + b\Phi \tag{2}$$

$$K_1 = (0.84 - 2.85\Phi)K_0 \tag{3}$$

4.2 Elastic-plastic stiffness

In Eq. (4), analytical elastic-plastic stiffness is

assumed to be modified from elastic stiffness by considering plastic deformation Δ_y and an attenuation coefficient γ. This is because the experimental force-deformation gradually becomes 'flat', once U-shaped bumpers yield, as shown in Fig. 5.

γ was obtained by data fitting analytical elastic-plastic stiffness to experimental stiffness from all 48 sets specimens. Figures 13 and 14 show the correlation between γ and Φ with different B under monotonic or cyclic load. γ were assumed to follow a normal distribution among all experimental data, and is independent to Φ and B. The significant coefficient of normality is 0.061, which is larger than 0.05. The mean value is 0.952 and the 95% confidence interval is (0.939, 0.967). The elastic-plastic stiffness can be updated by utilizing the mean γ as in Eq. (5).

$$K_2 = \gamma^{\Delta y} K_1 \tag{4}$$

$$K_2 = 0.952^{\Delta y} K_1 \tag{5}$$

4.3 Unloading stiffness

As seen in Fig. 5, the load-deformation unloading slope is slightly smaller than the elastic slope. θ is assumed to be the unloading stiffness attenuation coefficient to define unloading stiffness from elastic stiffness, $\theta = K_3 / K_1$.

θ was also obtained by data fitting experimental unloading stiffness from all the 48 sets of tested specimens, as shown in Figs. 15 and 16. It was observed that θ has a negligible relationship with Φ and B. The mean of the θ distribution is 0.845 while the 95% confidence interval is [0.810, 0.915] by assuming test results following a normal distribution. Analytical unloading stiffness can be defined as in Eq. (6).

$$K_3 = 0.845 K_1 \tag{6}$$

4.4 Experimental stiffness validation

Analytical stiffness equations (Eqs. (3), (5), (6)) were applied to predict the backbone curve for a different type of U-shaped bumper, with $t =$ 12 mm. As shown in Fig. 17, the analytical curves match with the experimental curves by considering peak experimental deformation input. Equations (3), (5), (6) could be used as an alternative method to calculate the stiffness of the U-shaped 65Mn steel bumper in a preliminary design phase.

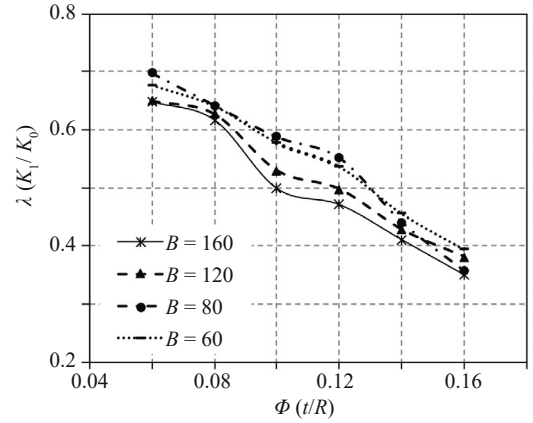

Fig. 11 λ and Φ curve under monotonic load

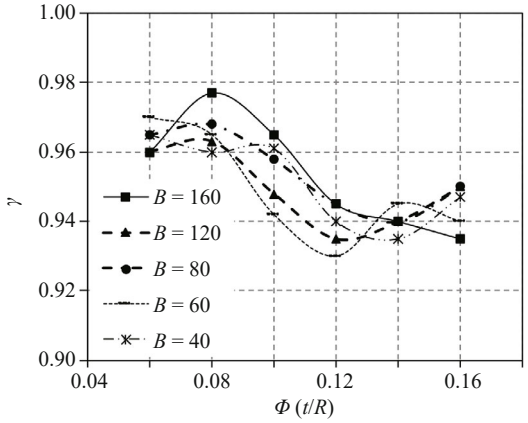

Fig. 13 γ and Φ curve under monotonic load

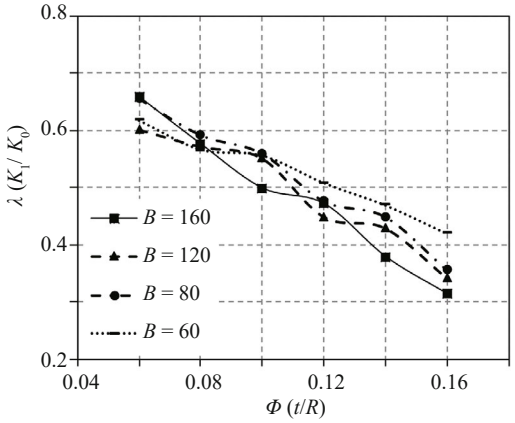

Fig. 12 λ and Φ curve under cyclic load

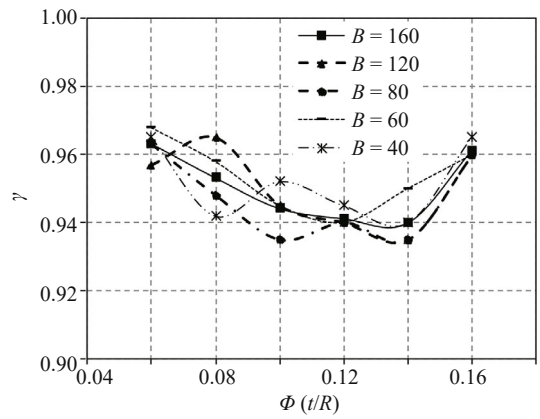

Fig. 14 γ and Φ curve under cyclic load

5 Analytical maximum elastic restoring force

5.1 Theoretical equation

The theoretical out-of-plane elastic restoring force of a U-shaped steel bumper was defined in an earlier study, as in Eq. (7) (Du *et al*., 2014). σ is principal tensile stress between the circular section and the straight section. From experimental tests on deformation and failure mechanism done in previous research (Han and Li, 2006; Cui, 2015), a U-shaped bumper reaches its elastic limit when σ equals to f_y with f_y representing the steel yield strength. The maximum elastic restoring force for a U-shaped 65Mn bumper is then modified to Eq. (8).

$$F = \frac{\sigma B t^2}{6R} \tag{7}$$

$$F_0 = \frac{f_y B t^2}{6R} \tag{8}$$

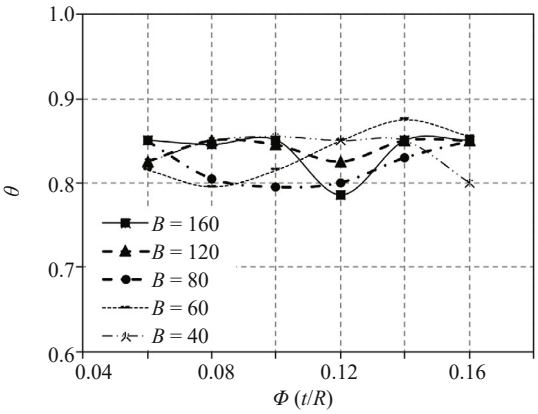

Fig. 15 θ and Φ curve under monotonic load

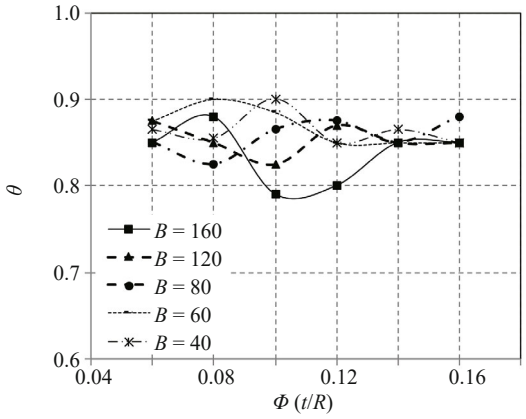

Fig. 16 θ and Φ curve under cyclic load

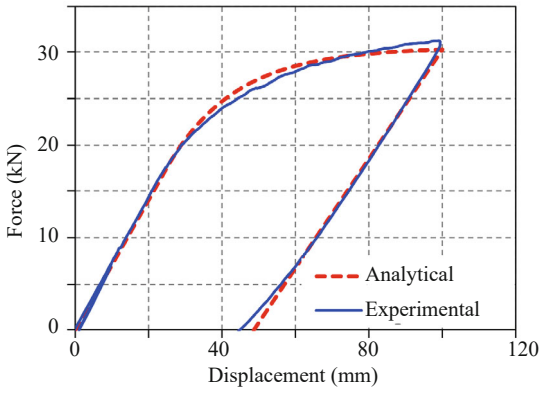

Fig. 17 Comparison of numerical fitting curve and test curve under monotonic load

5.1 Revised maximum elastic restoring force equation

The analytical maximum restoring forces calculated from Eq. (8) is larger than the experimental results from the tests of 48 sets. As a result, the analytical maximum elastic restoring force is modified in Eq. (9), while α is a correction coefficient. Figures 18 and 19 show that the experimental correlation among α , Φ, B is negligible. By following a normal distribution, the following statistical parameters are derived for α . The mean is 0.92, and the 95% confidence interval is (0.90, 0.94) when the significant coefficient is 0.053. The analytical maximum elastic restoring force can be redefined as in Eq. (10) by adopting the mean α .

$$F_1 = \alpha F_0 \tag{9}$$

$$F_1 = 0.92 \frac{f_y B t^2}{6R} \tag{10}$$

6 Applicability validation

The modification factors in Eqs. (3), (5), and (6) were obtained from U-shaped 65Mn steel bumpers, with R = 100 mm. To validate the applicability of these equations, 10 groups of bumpers (40 specimens in all) with a different R were tested under the same loading protocols. The design parameters are shown in Table 2.

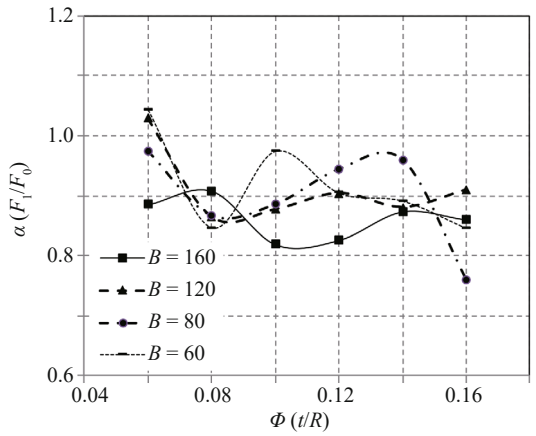

Fig. 18 α and Φ correlation under monotonic load

6.1 Validation of revised elastic stiffness, *R*

Figures 20 and 21 show the λ and Φ relation curves from Eq. (3) and the ten sets of experimental tests under both monotonic and cyclic loads. The analytical equation can accurately predict the λ value for U-shaped steel bumpers regardless of thickness and radius. In this study, the validation range for the factor Φ is [0.067, 0.2], which is the typical configuration for U-shaped steel bumpers.

6.2 Validation of other equations

Table 5 provides the experimental mean values of stiffness degradation factors γ from ten sets of specimens under monotonic and cyclic loading protocols. The analytical $\gamma = 0.952$ in Eq. (5) falls within the 95% confidence interval range defined by (0.939, 0.967). This proves the accuracy of Eq. (5) to predict elastic-plastic stiffness for U-shaped steel bumpers that have a Φ range from 0.067 to 0.2. Similarly, the analytical θ (0.845) in Eq. (6) closely matches the experimental mean of θ from the ten sets of specimens that are listed in Table 6. Within a 95% confidence interval (0.939, 0.967), the analytical θ was also proved to be practical and accurate. The experimental means of the maximum elastic restoring force correction coefficient α in Table 7 also demonstrates the accuracy of the analytical α (0.92) that is used in Eq. (10), when the 95% confidence interval for α is (0.90, 0.94).

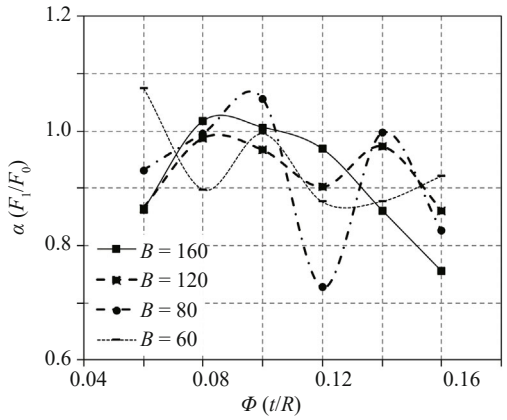

Fig. 19 α and Φ correlation under cyclic load

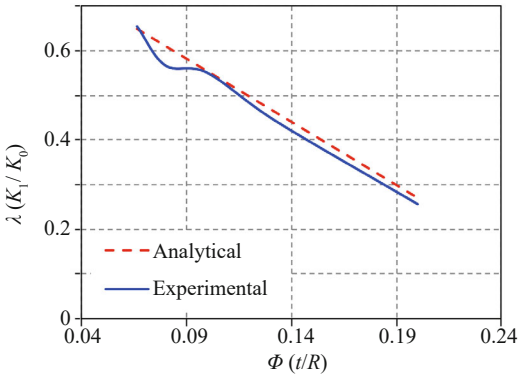

Fig. 20 Comparison of λ and Φ curve under monotonic load

7 Conclusion

In this study, a U-shaped 65Mn steel bumper was proposed as a novel displacement limitation device for base-isolated structures. Extensive experimental tests were conducted under monotonic and cyclic loading protocols to obtain the mechanical properties of U-shaped bumpers. With various design parameters, an analytical model to calculate the mechanical properties of the proposed bumpers was derived and validated by the experimental results. The main conclusions are as follows:

1. For U-shaped 65Mn steel bumpers, the surface strain between the circular section and the straight section increases significantly with bumper deformation. The surface strains are also observed to increase with Φ (the ratio of steel plate thickness to circular section radius, t / R) when the circular and straight sections have the same amount of deformation. Thus, a large Φ could develop visible plastic deformation in the circular portion. Also, bumper brittle fracture can be avoided by limiting Φ in the design phase.

Table 5 γ of U-shaped 65Mn steel bumpers with different *R*

	R (mm)	40	60	80	100	120
Loading	Monotonic	0.928	0.952	0.948	0.963	0.967
	Cyclic	0.932	0.954	0.950	0.959	0.969

Table 6 θ of U-shaped 65Mn steel bumpers with different *R*

	R (mm)	40	60	80	100	120
Loading	Monotonic	0.85	0.84	0.80	0.82	0.85
	Cyclic	0.85	0.85	0.75	0.83	0.90

Table 7 α of U-shaped 65Mn steel bumpers with different *R*

	R (mm)	40	60	80	100	120
Loading	Monotonic	0.88	0.97	0.91	0.83	0.94
	Cyclic	0.86	0.94	0.92	0.87	0.91

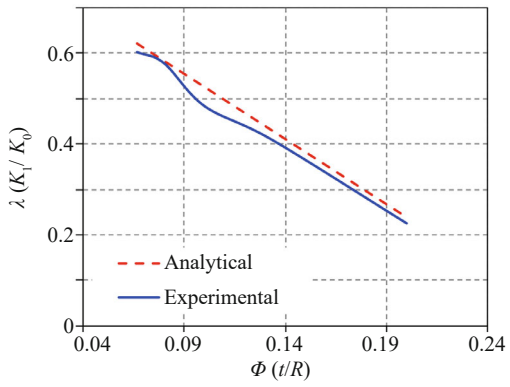

Fig. 21 Comparison of λ and Φ curve under cyclic load

2. The hysteretic loops of U-shaped 65Mn steel bumpers are rounded and symmetric, but also show pinching, which indicates that the ductility and energy dissipation capacity of the U-shaped 65Mn steel bumper is limited. However, the high yield strength of U-shaped 65Mn steel bumpers can efficiently reduce and limit the horizontal displacement of base-isolated structures in severe seismic events.

3. By comparing the results from the experimental tests and the proposed analytical equations regarding the mechanical properties of U-shaped 65Mn bumpers, it was found that the analytical equations can simulate the deformation properties and the maximum elastic restoring force with a high degree of accuracy. Those equations could provide a ready guidance for practical engineering design, when the design parameter Φ ranges from 0.067 to 0.2.

4. The geometric dimension of a U-shaped 65Mn bumper (e.g., straight section length (L), straight section width (B)) has a negligible effect on analytical modification factors, such as the elastic stiffness factor (λ), the stiffness reduction coefficient (γ), the unloading stiffness reduction factor (θ), and the maximum elastic restoring force correction coefficient (α).

References

Aiken I, Kelly J, and Tajirian F (1989), *Mechanics of Low Shape Factor Elastomeric Seismic Isolation Bearings*, Report No. UCB/EERC-89/13, University of California, Berkeley.

Cui X (2015), "Study on Mechanical Property of U-Shaped 65Mn Steel Plate Buffer and Soft Steel Damper," *M.S. Thesis*, Beijing University of Civil Engineering and Architecture, Beijing, China. (in Chinese)

Deng K, Pan P and Wang C (2013), "Development of Crawler Steel Damper for Bridges," *Journal of Constructional Steel Research*, **85**: 140–150.

Deng K, Pan P, Su Y and Xue Y (2015), "Shape Optimization of U-Shaped Damper for Improving Its Bi-Directional Performance Under Cyclic Loading," *Engineering Structures*, **93**: 27–35.

Dicleli M (2008), "Performance of Seismic-Isolated Bridges with and without Elastic-Gap Devices in Near-Fault Zones," *Earthquake Engineering and Structural Dynamics*, **37**(6): 935–954.

Du H and Han M (2014), "Impact and Energy Analysis of Deformation-Limited Base-Isolated Structure in Shaking Table Test," *Applied Mechanics and Materials*, **638-640**: 1811–1817.

Du H, Han M and Yan W (2014), "Study on the Calculation Method of Mechanical Characteristics for Constrained U-Shaped Steel Plates," *China Civil Engineering Journal*, **47**(S2): 158–163. (in Chinese)

Guerrein L and Azevedo J (1996), "Impact Problems on Base-Isolated Structures," *Proceedings of the 11th World Conference on Earthquake Engineering*, Acapulco, Mexico.

Han M and Li X (2006), "Testing Studies on Automatic Resilience of U-Shape Combination Buffers," *World Earthquake Engineering*, **22**(2): 110–113. (in Chinese)

Han M and Zhou X (1999), "Analysis of Soft-Collision Safety for Base Isolated Buildings," *Building Science*, **15**(1): 14–20. (in Chinese)

Ibarra L and Krawinkler H (2005), *Global Collapse of Frame Structures Under Seismic Excitations*, Report No. 29–51. Pacific Earthquake Engineering Research Center, Berkeley, CA.

Jiao Y, Kishiki S, Yamada S, Diana E, Konishi Y, Hoashi Y and Terashima M (2015), "Low Cyclic Fatigue and Hysteretic Behavior of U-Shaped Steel Dampers for Seismically Isolated Buildings Under Dynamic Cyclic Loadings," *Earthquake Engineering and Structural Dynamics*, **44**(10): 1523–1538.

Liu X, Li J and Chen X (2015), "Effects of X-Shaped Elastic-Plastic Steel Shear Keys on Transverse Seismic Responses of a Simply-Supported Girder Bridge," *Journal of Vibration and Shock*, **34**(2): 143–149. (in Chinese)

Masroor A and Mosqueda G (2012a), "Experimental Simulation of Base-Isolated Buildings Pounding Against Moat Wall and Effects on Superstructure Response," *Earthquake Engineering and Structural Dynamics*, **41**(14): 2093–2109.

Masroor A and Mosqueda G (2012b), "Impact Model for Simulation of Base Isolated Buildings Impacting Flexible Moat Walls," *Earthquake Engineering and Structural Dynamics*, **42**(3): 357–376.

Mavronicola EA, Polycarpou PC and Komodromos P (2017), "Spatial Seismic Modeling of Base-Isolated Buildings Pounding Against Moat Walls: Effects of Ground Motion Directionality and Mass Eccentricity," *Earthquake Engineering and Structural Dynamics*, **46**(7): 1161–1179.

Oh SH, Song SH, Lee SH and Kim HJ (2013), "Seismic Response of Base Isolating Systems with U-Shaped Hysteretic Dampers," *International Journal of Steel Structures*, **12**(2): 285–298.

Pant DR and Wijeyewickrema AC (2014), "Performance of Base-Isolated Reinforced Concrete Buildings Under Bidirectional Seismic Excitation Considering Pounding with Retaining Walls Including Friction Effects," *Earthquake Engineering and Structural Dynamics*, **43**(10): 1521–1541.

Polycarpou PC, Komodromos P and Polycarpou AC (2013), "A Nonlinear Impact Model for Simulating the Use of Rubber Shock Absorbers for Mitigating the Effects of Structural Pounding During Earthquakes," *Earthquake Engineering and Structural Dynamics*,

42(1): 81–100.

Skinner RL, Robinson WH and McVerry GH (1993), *An Introduction to Seismic Isolation*, John Wiley Sons Ltd., 268–269.

Suzuki K, Watanabe A and Saeki E (2005), "Development of U-shaped Steel Damper for Seismic Isolation System," *Nippon Steel Technical Report No. 92*, Tokyo, Japan.

Tagawa H and Gao J (2012), "Evaluation of Vibration Control System with U-Dampers Based on Quasi-Linear Motion Mechanism," *Journal of Construction Steel Research*, **70**: 213–225.

Wang Y and Ibarra L (2015), "Seismically Optimization of Modified Base-Isolated Systems for Next Generation Nuclear Structures," *Proceedings of the 23rd International Conference on Structural Mechanics in Reactor Technology*, Manchester, UK, August, 10–14.

Wang Y, Ibarra L and Pantelides C (2016), "Seismic Retrofit of a Three-Span RC Bridge with Buckling-Restrained Braces," *Journal of Bridge Engineering*, **21**(11): 04016073.

Wang Y, Ibarra L and Pantelides C (2019), "Collapse Capacity of Reinforced Concrete Skewed Bridges Retrofitted with Buckling-Restrained Braces," *Engineering Structures*, **184**: 99–114.

Xie X, Chen SX and Zhou X (2018), "A Simplified Analytical Model for U-Shaped Steel Dampers Considering Horizontal Bidirectional Deformation," *Bulletin of Earthquake Engineering*, **16**(12): 6243–6268.

Ye K, Li L and Zhu H (2009), "A Modified Kelvin Impact Model for Pounding Simulation of Base-Isolated Building with Adjacent Structures," *Earthquake Engineering and Engineering Vibration*, **8**(3): 433–446.

Zhou FL and Tan P (2018), "Recent Progress and Application on Seismic Isolation Energy Dissipation and Control for Structures in China," *Earthquake Engineering and Engineering Vibration*, **17**(1): 19–27.